Biophysical Journal Volume 108 March 2015 1380–1389

Article

Spectral Snapshots of Bacterial Cell-Wall Composition and the Influence of Antibiotics by Whole-Cell NMR

Rie Nygaard,[1] Joseph A. H. Romaniuk,[1] David M. Rice,[1] and Lynette Cegelski[1,*]
[1]Department of Chemistry, Stanford University, Stanford, California

ABSTRACT Gram-positive bacteria surround themselves with a thick cell wall that is essential to cell survival and is a major target of antibiotics. Quantifying alterations in cell-wall composition are crucial to evaluating drug modes of action, particularly important for human pathogens that are now resistant to multiple antibiotics such as *Staphylococcus aureus*. Macromolecular and whole-cell NMR spectroscopy allowed us to observe the full panel of carbon and nitrogen pools in *S. aureus* cell walls and intact whole cells. We discovered that one-dimensional ^{13}C and ^{15}N NMR spectra, together with spectroscopic selections based on dipolar couplings as well as two-dimensional spin-diffusion measurements, revealed the dramatic compositional differences between intact cells and cell walls and allowed the identification of cell-wall signatures in whole-cell samples. Furthermore, the whole-cell NMR approach exhibited the sensitivity to detect distinct compositional changes due to treatment with the antibiotics fosfomycin (a cell-wall biosynthesis inhibitor) and chloramphenicol (a protein synthesis inhibitor). Whole cells treated with fosfomycin exhibited decreased peptidoglycan contributions while those treated with chloramphenicol contained a higher percentage of peptidoglycan as cytoplasmic protein content was reduced. Thus, general antibiotic modes of action can be identified by profiling the total carbon pools in intact whole cells.

INTRODUCTION

Gram-positive bacteria such as *Staphylococcus aureus* surround themselves with a thick cell wall that is crucial to the mechanical and chemical integrity of the cell (1). The coordinated assembly of the cell wall is a tremendous microbial engineering feat that yields a micron-scale polymeric matrix, incorporating modified sugars and peptides. The rich history of research in examining cell-wall assembly processes is in part a result of the natural and intense curiosity to understand how such a self-assembly process occurs, is regulated, and is poised to respond to external stimuli and changes (2). At the same time, understanding cell-wall assembly and architecture is motivated by the need for new strategies to prevent and treat infectious diseases (3). This is particularly true with the dwindling number of antibiotics being added to the clinical arsenal of anti-infectives and is coupled to the increasing emergence of bacteria resistant to today's drugs of last resort such as methicillin- and vancomycin-resistant *S. aureus* (MRSA and VRSA) (1,4,5), so-called superbugs. As a human pathogen, *S. aureus* can cause skin and soft tissue infections as well as sepsis (6,7). Infection occurs when *S. aureus* penetrates skin or mucosal barriers and colonizes tissues or enters the bloodstream (6).

Cell-wall biosynthesis inhibitors are commonly used to treat *S. aureus* infections. These include penicillin, methicillin, and other β-lactams and cephalosporins, as well as the glycopeptide antibiotic vancomycin. In addition, oritavancin (Orbactiv; The Medicines Company, Parsippany, NJ) is a newer glycopeptide antibiotic that was approved by the FDA in August 2014 for the treatment of skin infections by Gram-positive bacteria including MRSA (8). Resistance to antibiotics appears inevitable with time and challenges us to develop new antibiotics in response to or in anticipation of antibiotic resistance (9). For antibiotics that target cell-wall biosynthesis, measurements of cell-wall composition and architecture are crucial to dissecting drug modes of action, and to characterizing changes as bacteria become resistant to an antibiotic. Yet, the Gram-positive cell wall is a heterogeneous insoluble macromolecular polymeric matrix that surrounds the cell and poses a challenge to nonperturbative analyses of composition and architecture. The primary component and structural scaffold of the cell wall is the peptidoglycan, composed of repeating units of a disaccharide-multipeptide building block that are polymerized and cross-linked to create a continuous network that envelops the cell (Fig. 1). Peptidoglycan biosynthesis is coordinated through the action of >10 proteins. Different cell-wall inhibitors target distinct steps in peptidoglycan biosynthesis, ranging from inhibiting the production of the disaccharide inside the cell (fosfomycin) (10) to preventing the cross-linking of peptide stems outside the cell (penicillin) (11,12). Wall teichoic acids and proteins are also covalently attached to the peptidoglycan to generate a complete cell wall that protects the cell from turgor pressure and external stress and confers functional

Submitted December 15, 2014, and accepted for publication January 13, 2015.

*Correspondence: cegelski@stanford.edu

Rie Nygaard and Joseph A. H. Romaniuk contributed equally to this work.

Editor: Francesca Marassi.

0006-3495/15/03/1380/10 $2.00

http://dx.doi.org/10.1016/j.bpj.2015.01.037

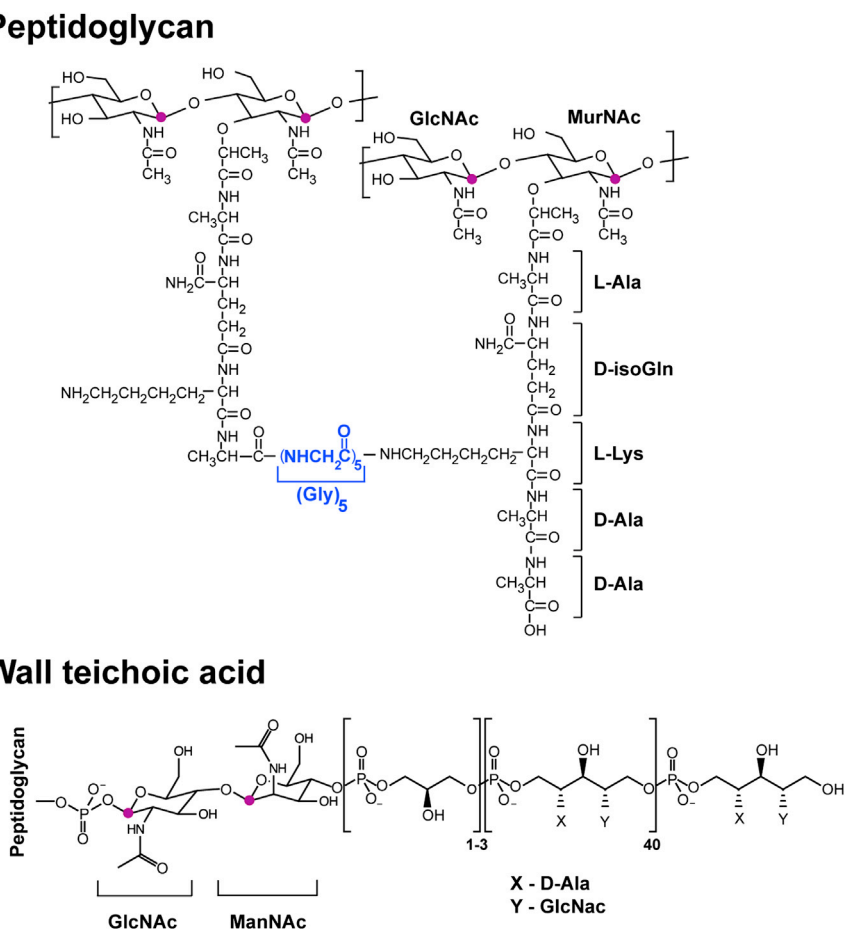

FIGURE 1 Chemical structures of major cell-wall components: peptidoglycan and wall teichoic acid. The primary component and structural scaffold of the cell wall is the peptidoglycan (*top*), comprised of repeating units of a disaccharide-multipeptide building block. Subunits composed of the disaccharide, pentapeptide stem, and pentaglycine bridge attached to the ε-amino group of L-lysine are assembled inside the cell and then transported to the cell surface. Peptide stems without glycine bridges can also be transported (25,43,44). After transport to the cell surface, the sugars are polymerized through transglycosylation and the peptides are cross-linked through transpeptidation (bond-formation between D-Ala and Gly, resulting in the concomitant loss of the terminal D-Ala). Wall teichoic acids are also covalently attached to the peptidoglycan (*bottom*). To see this figure in color, go online.

benefits in adhesion and host interactions during infection (13,14).

Solid-state NMR has emerged as a powerful technique to examine the chemical composition and architecture of cell walls in bacteria as well as in plants. The quantification of key cross-linking sites has been performed in both isolated bacterial cell walls and in whole cells (15,16) using appropriate biosynthetic labeling strategies and NMR detection. A decrease in the D-Ala-Gly cross-link density, for example, can be detected in cells treated with penicillin (16), which leads to a weakened cell wall and subsequent cell lysis. Although the modes of action of penicillin and many other antibiotics have been examined extensively during and after the Golden Age of antibiotics in which most antibiotics were discovered, the conventional analytical methods typically require enzymatic or acid hydrolysis of polymer units and then rely on subsequent quantification estimates by chromatography and mass spectrometry of the units that are able to be solubilized (17). Complications in quantification arise from the incomplete dissolution of the cell wall and from differences in the extent of detection of certain substituents based on charge and properties that influence ionization in mass spectrometric detection, for example. Solid-state NMR approaches permit the analysis of cell-wall composition in intact cell walls and, for certain elements, in whole cells themselves. NMR methods were used previously to examine the influence of vancomycin on cell-wall composition (15) and to determine the mode of action of the recently FDA-approved oritavancin (Orbactiv; The Medicines Company) by examining changes among key peptidoglycan cross-links and peptidoglycan precursors (18). Specific internuclear distance measurements using rotational-echo double resonance (REDOR) NMR were also employed to develop atomic-level models of antibiotic-cell wall complexes, particularly for oritavancin and related analogs, and permitted the generation of structure-activity relationships to correlate antibiotic efficacy with structural mapping in the cell wall (18–23). All of these studies were performed using selectively labeled samples to identify key nuclei of interest. Cross-links were identified and quantified, for example, by incorporating D-[1-^{13}C]Ala and [^{15}N]Gly, whereas [1-^{13}C]Gly and [ε-^{15}N]Lys labeling has been used to quantify bridgelinks. Indeed, many studies with selectively labeled samples have provided important insights regarding specific features of cell-wall composition, architecture, and drug modes of action.

Here, we report our discoveries and valuable spectroscopic signatures using unlabeled and uniformly labeled

samples that report on all carbon and nitrogen pools in an unbiased way. Uniform labeling is typically simpler to implement than selective labeling strategies, where one must consider and quantify the isotopic enrichment and extent of scrambling or isotopic dilution attributed to endogenous synthesis. We define and compare the ^{13}C and ^{15}N composition of intact *S. aureus* whole cells and cell walls using cross-polarization magic-angle spinning (CPMAS), REDOR, frequency-selective REDOR, and two-dimensional ^{13}C spin-diffusion measurements. There are clear differences between the NMR spectra of cell walls and the whole cells from which they were isolated that immediately reveal the compositional differences in their carbon and nitrogen pools. We also discovered that changes in cell-wall composition in protoplast preparations and among antibiotic-treated cells could be identified in intact whole-cell samples. This approach to examining intact cell walls and whole cells by NMR provides spectral snapshots of cell-wall composition in the spirit of how whole-cell biochemical assays such as Western blots can reveal the comparative levels of specific soluble proteins of interest among cell lysates. As new discoveries are being made regarding the full extent of modes of action of even some of our classic antibiotics such as penicillin and other β-lactams, more holistic and less perturbative methods are invaluable in fully understanding the influence of antibiotics on cellular processes (24).

MATERIALS AND METHODS

Growth of *S. aureus* and isolation of peptidoglycan

Uniformly labeled *S. aureus* (ATCC No. 29213; American Type Culture Collection, Manassas, VA) were grown in a modified *S. aureus* synthetic medium (SASM) (15,25,26) in which all amino acids were replaced by 2 g/L ^{15}N labeled algal amino-acid mixture or ^{15}N and ^{13}C labeled algal amino-acid mixture (Cat. No. 487910; ISOTEC, Sigma-Aldrich, St. Louis, MO). The algal extract contains between 65 and 95% amino acids by mass and has an isotope enrichment of 99% for ^{13}C and ^{15}N. For uniformly ^{15}N- and ^{13}C-labeled samples, $(^{15}NH_4)_2SO_4$ (98% ^{15}N enrichment) and [u-^{13}C] glucose (99% ^{13}C enrichment) were also used, respectively, in place of their unlabeled counterparts. For cells treated with antibiotics, each antibiotic was added during *S. aureus* growth in the modified SASM at OD_{660} = 0.5 and cells were harvested 270 min later.

The *S. aureus* cultures were maintained on TSA (tryptic soy agar). To begin NMR sample preparations, 5 mL aliquots of [^{15}N]SASM or [^{13}C, ^{15}N]SASM were inoculated with a single colony and grown overnight at 37°C, shaking at 200 rpm. For whole-cell and cell-wall preparations, 300 mL cultures were prepared in 1 L flasks by inoculating the SASM broth with 1 mL (a 1:300 dilution, v/v) of the overnight starter culture. Whole-cell samples were prepared from 300 mL cell culture and cell-wall samples were prepared from 900 mL of cell culture. Cells were harvested at OD_{660} = 1.0 by centrifugation at 10,000 *g* at 4°C for 10 min. Cells were subsequently washed three times by resuspension with 5 mM HEPES buffer (pH 7) and centrifugation to remove excess media components. For whole-cell samples, the final cell pellets were frozen and lyophilized. The isolation of cell walls was performed as described previously in Zhou and Cegelski (25).

Protoplast preparation

The *S. aureus* protoplasts were prepared following literature protocols. Cultures were grown to OD_{660} = 1.0 in u-^{13}C, ^{15}N SASM and the cells were isolated by centrifugation at 10,000 *g* at 4°C for 10 min, and washed once with 50 mM Tris (pH 7.5). The cells were suspended in 1 M trehalose and 50 mM Tris, and allowed to equilibrate on ice. A quantity of 3 mg of lysostaphin (Sigma-Aldrich) and 1 mg of DNaseI (Sigma-Aldrich) were then added to the suspension, allowed to equilibrate, and then incubated at 37°C, 200 rpm for 1 h. The digestion of the cell walls and preparation of the protoplasts was judged complete when the optical density of a 1:4 dilution of the suspension in 50 mM Tris decreased from 1.0 to 0.25, indicating cell lysis. The protoplasts were then collected by centrifugation at 10,000 *g* at 4°C for 30 min, and washed once with the buffered 1 M trehalose solution. The isolated protoplasts were frozen and lyophilized.

Solid-state NMR

Solid-state NMR experiments were performed in an 89-mm 11.7 T wide-bore magnet (Agilent Technologies, Danbury, CT) using a four-frequency HPCN transmission-line probe (^1H 500.92 MHz, ^{13}C 125.96 MHz, and ^{15}N 50.76 MHz) with a four-channel DD2 console (Agilent Technologies), employing high-power, active transmit/receive switching. Samples were spun at 7143 Hz in thin-wall 5-mm zirconia rotors and maintained at a temperature of ~5°C (with an FTS Chiller, from FTS Thermal Products, SP Scientific, Warminster, PA, supplying air at −25°C). Spectra were obtained with ^1H-^{13}C CPMAS, followed by synchronized spin-echo detection after two rotor periods. Field strengths for ^{13}C and ^{15}N cross-polarization were all 50 kHz with π-pulses of 10 μs and with a 10% linear ^1H ramp centered at 57 kHz. Decoupling field strengths were 72 kHz (using SPINAL) during acquisition and 100 kHz (continuous wave) during periods containing REDOR pulses. The CPMAS mixing time was 1.5 ms and the recycle time was 3.0 s for all experiments. ^{13}C chemical shifts were referenced to tetramethylsilane as 0.0 ppm using a solid adamantane sample at 38.5 ppm. The ^{15}N chemical shift scale is referenced to ammonia as 0 ppm where solid L-[amide-^{15}N]Asn appears at 114.5 ppm. Referencing of ^{15}N to ammonia at 0 ppm is a change from our previous use of solid NH_4SO_4 at 0 ppm typical in the older solid-state NMR literature and corresponds to a difference of 25.4 ppm for ^{15}N chemical shifts.

REDOR was used to restore the ^{13}C-^{15}N dipolar couplings that are removed by magic-angle spinning (MAS). REDOR experiments are always done in two parts, once with dephasing (S) and once without (full echo, S_0). The difference in signal intensity (REDOR difference, $\Delta S = S_0 - S$) for the observed spin in the two parts of the REDOR experiment is directly related to the corresponding distance to the dephasing spin. Standard REDOR (27) for Fig. 3 made use of alternating π-pulses on the ^{13}C and ^{15}N channels with XY8 phase cycling followed by echo detection. The 16-T_r frequency-selective REDOR measurement in Fig. 4 made use of the general method of Jaroneic et al. (28), although we employed alternating pulses on both ^{15}N and ^{13}C channels with XY8 phase cycling because ^{13}C was at natural abundance. Simultaneous refocusing and inversion pulses on the ^{13}C observe and ^{15}N dephasing channels, respectively, were placed in the center of the total evolution period. A selective RNSOB pulse (29) (1960 μs centered in 16 rotor periods) was used for ^{15}N inversion in the center of the sequence, whereas a nonselective pulse of 10 μs was used to refocus the entire ^{13}C spectrum. The bandwidth of the ^{15}N inversion pulse was verified with a selective inversion centered between two $\pi/2$ pulses.

Two-dimensional ^{13}C spectroscopy for Fig. 5 was performed with a standard hXX method (30) using dipolar-assisted rotational resonance (DARR) mixing (31) (^1H 7.1 kHz). We note that at the 7143 Hz spinning speed employed here, DARR and proton-driven spin diffusion (32) have nearly the same mixing rate, so the ^1H irradiation is not strictly necessary for further experiments. Projections for Fig. 4 were obtained by summing F2 traces over the appropriate frequency region of F1.

RESULTS

Carbon and nitrogen pools in whole cells and cell walls

Uniformly labeled cells were prepared using a modified SASM. Unlike *Escherichia coli*, *S. aureus* cannot grow on a minimal medium with only general nitrogen and carbon sources for growth and require several amino acids and vitamins to be provided exogenously (33). SASM includes all 20 amino acids plus vitamins, trace metals, etc., and has been used to introduce specific amino-acid labels in cells and cell walls (26). We substituted the 20 amino acids with a commercially available ^{15}N-labeled- or ^{15}N/^{13}C-labeled amino-acid algal extract. For uniform ^{13}C and ^{15}N labeling, $(^{15}NH_4)_2SO_4$ and [$^{13}C_6$]glucose were also used, respectively, in place of their unlabeled counterparts in SASM.

The ^{13}C CPMAS spectra of [u-^{13}C, u-^{15}N] whole cells and cell walls contain a prominent carbonyl peak centered at 172 ppm and an array of peaks associated with polysaccharides, protein α-carbons, and aliphatics (Fig. 2). The sharper peak at 33 ppm in the whole-cell spectrum is indicative of lipid content and the 140–160 ppm peaks correspond to nucleic acids, e.g., ribosomal RNA. Nucleic acids and lipids should be and are absent in the cell-wall spectrum, confirming that unbroken cells were removed during the isolation of cell walls (25). Glycine comprises approximately half the peptide pool in the cell-wall sample and the increased intensity of the glycine α-carbons at 42-ppm relative to other α-carbons is evident in the cell-wall spectrum versus the whole-cell spectrum.

The ^{15}N CPMAS spectral differences are dramatic and also reveal the major compositional differences between whole cells and cell walls. Whole cells, with their collection of cytoplasmic and membrane proteins, ribosomal RNA, lipids, and cell walls, contain amides ascribed to peptide backbones, Gln and Asn side-chain nitrogens, and other amide-containing species. They also contain side-chain nitrogens associated with histidines, arginines, and lysines (Fig. 2). The cell walls, in contrast, do not harbor the full panel of amino acids observed in whole cells. The ^{15}N cell-wall spectrum contains only amide contributions, indicating the full extent of bridge-linking and cross-linking in this sample, with minimal open (non-cross-linked) glycine bridges or lysyl amines present, and, as expected, no histidine or arginine contributions.

Carbon-nitrogen one-bond pairs in whole cells and cell walls

The general α-carbon and nitrogen amide assignments indicated in Fig. 2 are further supported and characterized experimentally in Figs. 3 and 4. In Fig. 3, ^{13}C[^{15}N] REDOR was employed using a ^{15}N-enriched sample to identify carbons in whole cells and cell walls that are directly bonded to nitrogen (Fig. 3), where REDOR restores the ^{13}C-^{15}N dipolar couplings that are removed by magic-angle spinning. REDOR is powerful when applied in this way as a

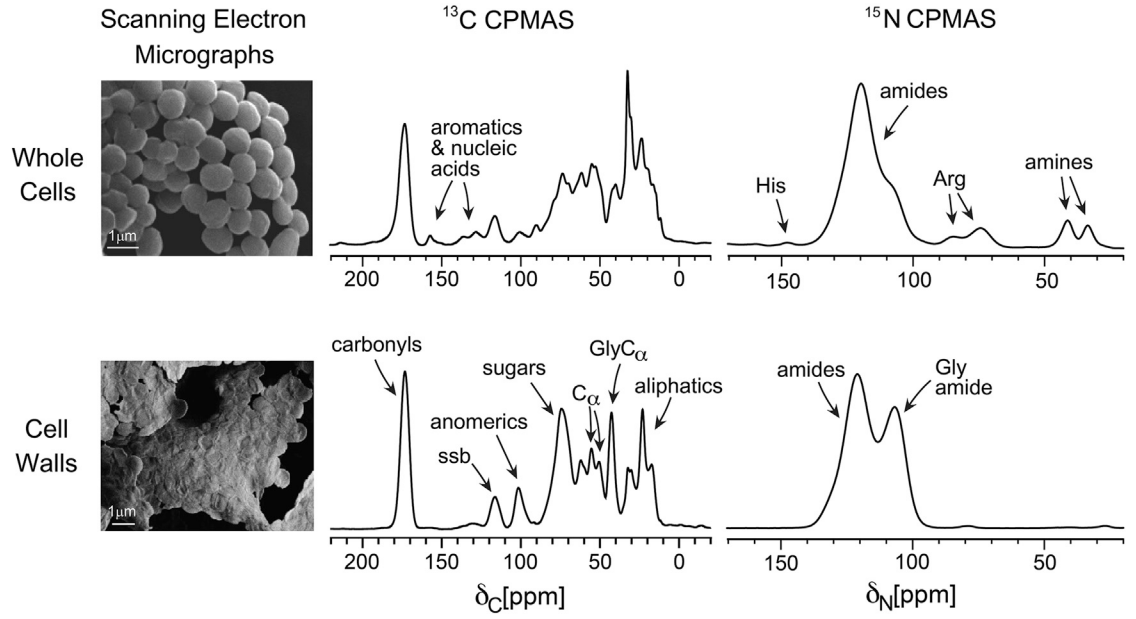

FIGURE 2 Comparative CPMAS spectra of whole cells and cell walls. The ^{13}C and ^{15}N CPMAS spectra of [u-^{13}C, u-^{15}N]-labeled *S. aureus* whole cells (grown to $OD_{600} = 1.0$) and cell walls isolated from these cells. Whole-cell spectra contain more types of carbon and nitrogen resonances than cell walls, including the full panel of amino acids, RNA, and lipids. The high prevalence of glycine in the cell wall is revealed in the α-carbon region of the ^{13}C spectrum as well as in the ^{15}N cell-wall spectrum, as annotated. The whole-cell and cell-wall samples were 66 and 60 mg, respectively. In total, 1024 scans were collected for ^{13}C and 12,288 for ^{15}N.

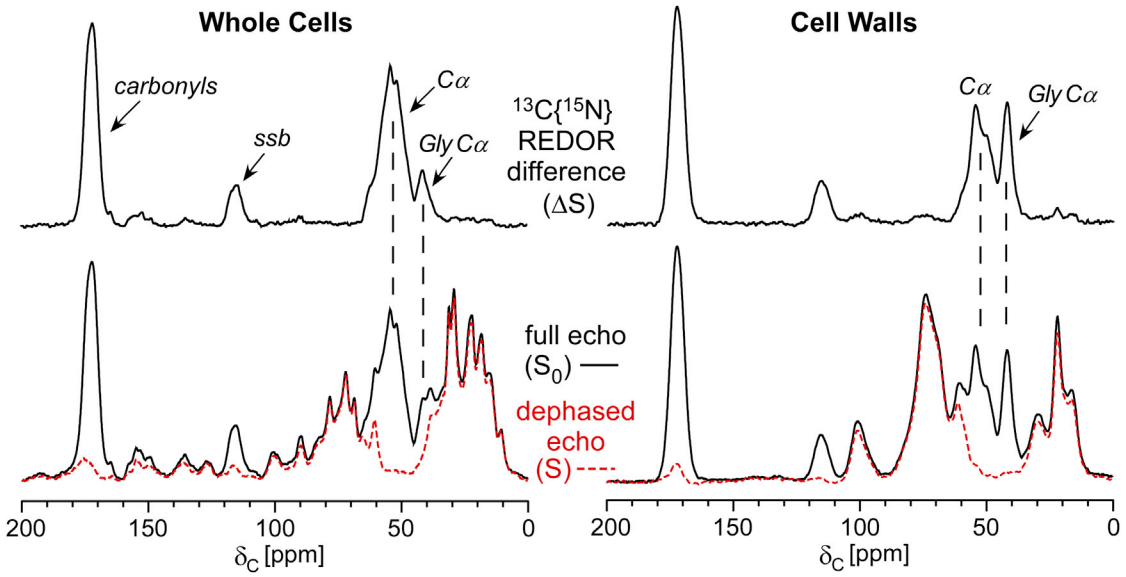

FIGURE 3 $^{13}C\{^{15}N\}$ REDOR of *S. aureus* whole cells and cell walls. The $^{13}C\{^{15}N\}$ REDOR NMR performed for 1.68 ms (12 T_r) of [u-^{15}N]-labeled whole cells and cell walls reveals directly bonded ^{13}C-^{15}N pairs, primarily due to peptide bonds and α-carbons. Each dephased spectrum (*dashed line*) is provided as an overlay with the S_0 full-echo spectrum (*solid line*). The difference spectrum (ΔS) represents the exact difference of the S_0 and S spectra and shows just the carbons that were selected through their one-bond dipolar coupling to nitrogen. The carbonyl spinning sideband is indicated by *ssb*. A total of 16,384 scans of S_0 and S were collected for the whole-cell sample (57 mg) and cell-wall samples (35 mg). To see this figure in color, go online.

spectroscopic filter to identify carbons, for example, that are one-bond or other specified distance away from another nucleus. In whole cells, the carbonyl peak is nearly completely dephased after 1.68 ms (12 T_r with 7143 Hz MAS) of $^{13}C\{^{15}N\}$REDOR dephasing (Fig. 3). At this evolution time, one-bond C-N couplings would exhibit complete dephasing. This result is consistent with most of the carbonyl contributions in whole cells arising from proteins, where peptide carbonyls completely dephase. Nucleic acid carbons are also dephased in the 140–160 ppm region and the protein α-carbons ranging from 40 to 70 ppm are dephased by nitrogen. Cell walls lack nucleic acids, but are rich in the peptidoglycan peptides described above. The 42-ppm peak in the cell-wall spectrum is uniquely attributed to glycyl α-carbons and is completely dephased, but exhibits only 70% dephasing in whole cells, indicating that other whole-cell carbons not bonded to a nitrogen also contribute to the 42-ppm carbon shift in a whole-cell

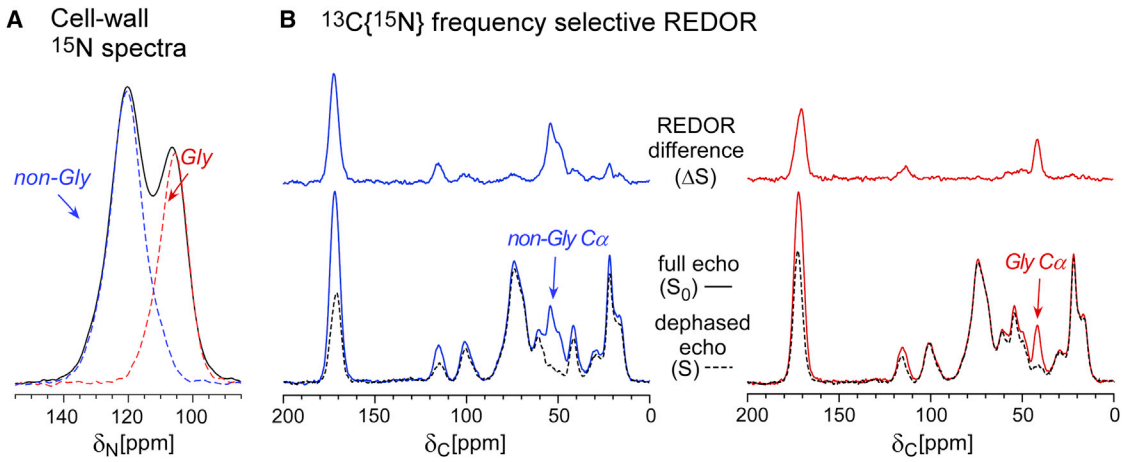

FIGURE 4 Frequency-selective REDOR for spectral correlations in cell walls. (*A*) Frequency-selective ^{15}N pulses select each of two amide peaks in the ^{15}N CPMAS spectrum. (*B*) Frequency-selective ^{15}N dephasing pulses were used in 16-T_r (2.24 ms)$^{13}C\{^{15}N\}$ REDOR measurements to experimentally confirm the spectral assignments made in Fig. 2. Recoupling with the up-field ^{15}N peak at 120 ppm results in dephasing of carbonyls and preferential dephasing of the α-carbons centered at 55 ppm, attributed to α-carbons other than glycine (*left*, *blue REDOR spectra*). Recoupling with the down-field ^{15}N peak centered at 107-ppm results in preferential dephasing of the 42-ppm glycine α-carbons (*right*, *red REDOR spectra*). A total of 8192 scans of S_0 and S were collected for each set of spectra of cell walls (35 mg). To see this figure in color, go online.

spectrum. Thus, the cell-wall REDOR spectra identify the one-bond C-N pairs as arising from carbonyls (corresponding to peptide bonds and *n*-acetylated glycosyl moieties) and peptide α-carbons.

Frequency-selective NMR experiments were performed to experimentally demonstrate and emphasize the glycine-specific contributions to the cell-wall ^{13}C and ^{15}N spectra. The glycine α-carbon has a unique chemical shift that can be utilized for spectroscopic selection strategies in complex whole-cell systems (15,32). When involved in a peptide bond, the glycine nitrogen chemical shift is also distinct from other amides and we demonstrated using frequency-selective REDOR that the up-field ^{15}N shift at 107 ppm arises primarily from glycyl nitrogens, whereas the lower field ^{15}N peak near 120 ppm is associated with nonglycine α-carbons (Fig. 4 *A*). In frequency-selective REDOR experiments, carbons were observed at natural abundance and nitrogens that were uniformly labeled were selectively dephased to recouple only the nitrogens near 107 or 120 ppm, as indicated in Fig. 4. The nonglycine α-carbons were preferentially dephased when recoupling was performed by selectively dephasing the 120-ppm ^{15}N resonance associated with the general amide pool (Fig. 4 *B*, *top*, *blue*), whereas the glycine α-carbon peak was selectively dephased by nitrogens at 107 ppm (Fig. 4 *B*, *bottom*, *red*). Polysaccharide signatures identify cell-wall content in whole cells

We hypothesized that the anomeric and sugar carbons in whole-cell spectra largely arise from cell-wall sugars in the peptidoglycan and teichoic acids. In addition to these contributions, the whole cells would contain lipoteichoic acid and some metabolic sugar pools destined for the cell-wall and modified lipid biosynthetic pathways. We used ^{13}C-^{13}C DARR to identify carbons that are near to one another in cell walls and whole cells. Assignments of cell-wall carbons (*red*) are provided in Fig. 5. The distinct amino acids that comprise the peptidoglycan can be assigned, including their carbonyl and α-carbons in addition to some side-chain carbons, and the sugar system can be identified in the 55–105 ppm region. The assigned two-dimensional cell-wall spectrum is provided as an overlay atop the whole-cell spectrum, for which there are numerous cellular contributions that cannot be uniquely assigned. To assess the similarity of the sugar spin systems in the two samples, a spectral slice of each two-dimensional plot corresponding to carbons that arise from proximity to the 100-ppm anomeric carbons is provided at the top of the figure. We found that DARR can be employed in this way to detect the polysaccharide spin system in whole cells and reveals similar sugar peaks as in an isolated cell-wall sample.

Detection of reduced cell-wall content in protoplasts

To manipulate and further examine the sugar-carbon spectral pools, we prepared a protoplast sample that consists of intact cells with only a thin layer of cell wall surrounding the cell after the majority of the peptidoglycan is digested with lysostaphin. Protoplasts were stabilized by trehalose to prevent cell lysis. Sucrose is often used as an osmotic stabilizer in protoplast preparations, but trehalose is a suitable substitute and avoids unwanted spectral overlap in the 100-ppm region where sucrose carbons would appear. Instead, trehalose carbons contribute to peak intensity primarily at 92 and 73 ppm with smaller contributions at 68, 62, and 61 ppm (Fig. 6). Digestion of peptidoglycan with lysostaphin results in protoplasts that have a ^{13}C spectrum with an obvious reduction in anomeric carbons, where the whole-cell and protoplast spectra have been normalized by overall integrated area (Fig. 6). A concomitant decrease in sugar carbons is observed between 60 and 85 ppm and a decrease in carbons at 42 ppm is consistent with the loss of glycine, which is prevalent in the cell wall. As revealed in the comparative $^{13}C\{^{15}N\}$REDOR spectra of whole cells and cell walls in Fig. 3, whole cells contain additional non-Gly contributions between 40 and 45 ppm and these are not altered. In addition, the trehalose used to protect the protoplasts contributes to the spectrum at 90 ppm and precludes this region from being used for comparison. The spectra are normalized by total integrated area and give the same result when normalized by sample mass and number of scans. The carbonyl peak intensity contributes similarly to whole cells and to cell walls by mass, and thus no difference is observed in protoplasts with reduced cell-wall content. This comparison is sensitive to compositional parameters that differ between two samples. Overall, the loss of cell wall that results during a protoplast preparation can be observed in the comparative ^{13}C CPMAS spectra of whole cells and protoplast preparations.

Antibiotic-induced alterations in cell-wall composition by whole-cell NMR

We tested the sensitivity of the approach described above to detect cell-wall alterations in whole cells due to antibiotic treatment. Untreated cells were compared to cells treated with fosfomycin and chloramphenicol. Fosfomycin is a cell-wall biosynthesis inhibitor that inactivates the enzyme MurA, responsible for the ultimate ability to link soluble peptide and glycan components inside the cell to generate cell-wall precursors (10,34,35). Chloramphenicol has an entirely different mode of action and targets the bacterial ribosome to generally inhibit cellular protein synthesis by interfering with peptidyl transferase activity (36–38). Compared to untreated cells, fosfomycin treatment resulted in notable carbon pool decreases among all polysaccharide carbons in the 55–100-ppm range. A reduction in the 38-ppm shoulder of the broader peak centered at ~42 ppm is consistent with decreased glycine content (Fig. 7). Chloramphenicol treatment, in contrast, does not inhibit cell-wall

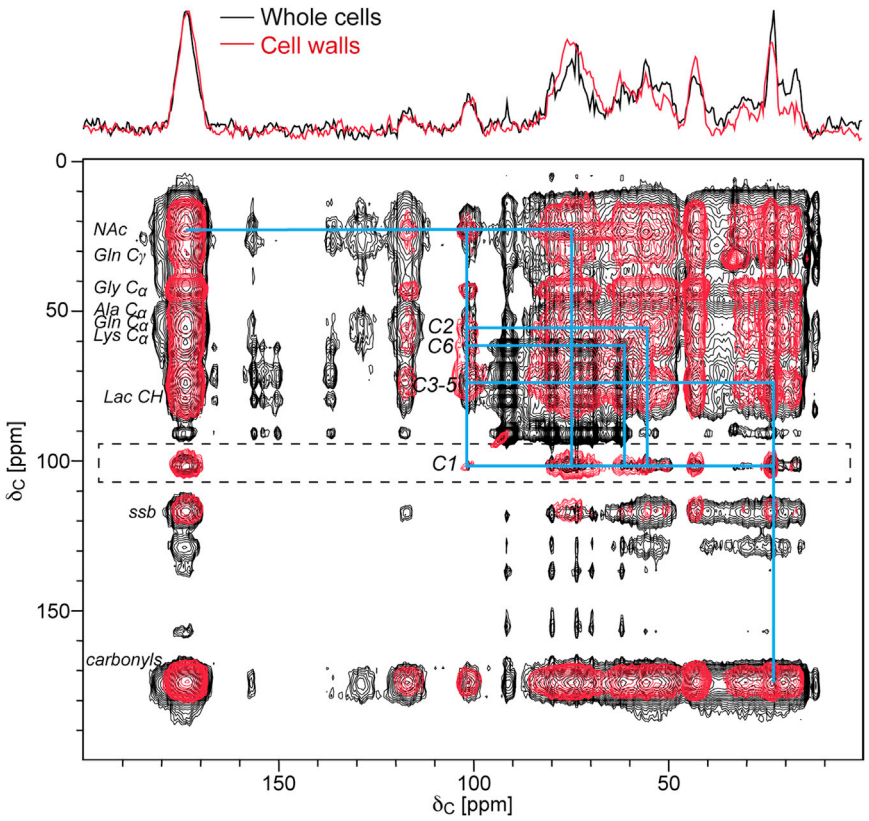

FIGURE 5 Comparative polysaccharide correlations in whole cells and cell walls. A two-dimensional ^{13}C-^{13}C DARR spectrum was obtained for [u-^{13}C, u-^{15}N]-labeled whole cells and cell walls using a spin-diffusion mixing time of 2 s. Assignments are based on the chemical shifts reported by Kern et al. (45) and in the Biological Magnetic Resonance Bank. The ^{13}C-^{13}C DARR measurement was also performed on whole cells (*black*) and is compared to the cell-wall spectrum (*red*) with the same mixing time of 2 s. The whole-cell two-dimensional spectrum contains more contributions from all the carbon types in proteins and other molecules, observed as additional peaks and broader peaks than in the cell-wall spectrum, in addition to the cell-wall contributions. Comparison of the whole-cell (*black*) and cell-wall (*red*) one-dimensional traces identifies the detected carbons that arise from spin-diffusion starting at the anomeric carbon at 100 ppm, and demonstrates the similar environment of the anomeric carbons, arising from the cell wall whether detected in isolated cell walls or intact cells. These data were acquired using the same samples as in Fig. 2, with 84 scans for the cell walls (60 mg) and 192 scans for whole cells (66 mg), each with 128 increments in the second dimension. To see this figure in color, go online.

synthesis, but instead prevents protein synthesis at the ribosome (36). The chloramphenicol-treated NMR spectrum reveals the relative increase in cell-wall content in this whole-cell sample, as protein synthesis is not maintained to keep up with the demands of the cell during chloramphenicol treatment. Thus, the cell-wall carbons represent a higher percentage of the whole-cell carbon pools after treatment with chloramphenicol.

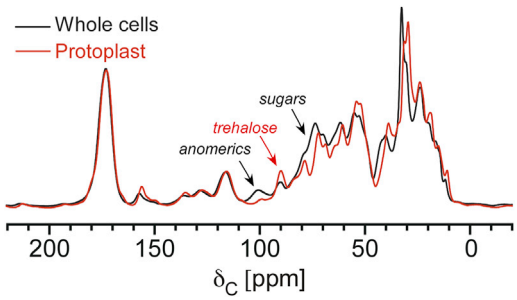

FIGURE 6 ^{13}C CPMAS spectrum of intact protoplasts reveals decreased cell-wall content. The ^{13}C spectra of protoplasts reveal a major decrease in the anomeric carbons in the protoplast sample at 100 ppm relative to the parent whole-cell spectrum. A decrease in the cell-wall sugar region from 60 to 85 ppm is also observed and the decrease in intensity at 38 ppm is consistent with the loss of glycyl α-carbons, where glycyl residues comprise ~50% of the amino acids in the peptidoglycan. Trehalose, used as an osmotic stabilizer of protoplasts, contributes significantly to peak intensity at 92 and 73 ppm with smaller contributions at 68, 62, and 61 ppm. In total, 1024 scans were collected for the whole-cell (66 mg) and protoplast (71 mg) samples. To see this figure in color, go online.

DISCUSSION

The ability to obtain quantitative comparisons of chemical and molecular composition is crucial for problem-solving efforts in biology and biochemistry. Quantitative comparisons of specific proteins can be profiled among intact cellular preparations as well as processed extracts by immunoblotting and ELISA assays. RNA transcripts can be enumerated after RNA isolation. Quantitative profiling of peptidoglycan and other macromolecular and polymeric species, e.g., lipids and polysaccharides, however, pose more of a challenge to analysis by conventional methods. In particular, characterizing the peptidoglycan composition in Gram-positive bacteria such as *S. aureus* is more challenging than in *E. coli* due to the presence of a more highly cross-linked network (39). Enzymatic digestions followed by HPLC-MS analyses (17,40–42) can provide some valuable information about the qualitative composition of the peptidoglycan, but does not provide a complete accounting of peptidoglycan components. The highly cross-linked muropeptide species that cannot be fully digested and resolved often appear as a hump in HPLC chromatograms (40). We sought to develop a new approach to examine intact cell walls and whole cells by NMR that

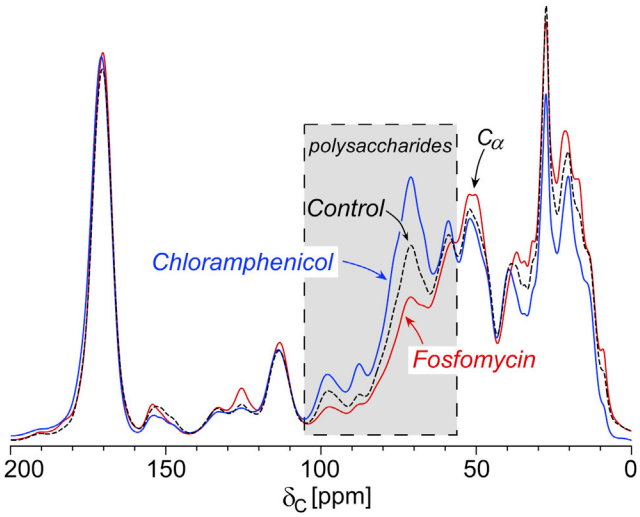

FIGURE 7 Whole-cell NMR spectra reveal antibiotic-induced alterations in cell-wall content. Fosfomycin targets cell-wall biosynthesis in *S. aureus*, whereas chloramphenicol is a protein synthesis inhibitor. ^{13}C CPMAS spectra of whole cells harvested after fosfomycin treatment (40 μg/mL) revealed decreased cell-wall content as assessed by the diminution of the anomeric and polysaccharide carbon peaks with respect to other carbons in the spectrum. In contrast, chloramphenicol treatment (20 μg/mL) results in enhanced cell-wall content relative to the overall whole-cell carbon pools with reduced cytoplasmic protein contributions. Spectra were normalized by integrated intensity to emphasize the relative increases and decreases among all types of carbons in the three samples. Although this normalization is the most intuitive, the conclusions do not change if the spectra are normalized by carbonyl or aromatic or aliphatic carbon intensity. A total of 1024 scans were acquired for the control (51 mg), fosfomycin (59 mg), and chloramphenicol-treated (56 mg) samples. Antibiotics were added at $OD_{660} = 0.5$ and cells were harvested 4.5 h after antibiotic addition. Final OD_{660} values were 2.8 (control), 1.4 (fosfomycin), and 1.6 (chloramphenicol). To see this figure in color, go online.

could provide spectral snapshots of cell-wall composition and content in the spirit of how whole-cell biochemical assays such as Western blots can reveal the comparative levels of specific proteins of interest. We avoided selective amino-acid labeling strategies that require determinations of enrichment, and label scrambling, in order to make quantification straightforward and to introduce a method that could be readily extended to other organisms. Thus, ^{13}C spectra were obtained from *S. aureus* cells with ^{13}C enrichments levels either at natural abundance or fully labeled at 99%. When performing ^{15}N NMR measurements, samples were uniformly ^{15}N labeled.

We discovered that simple one-dimensional ^{13}C and ^{15}N spectra of whole cells and cell walls reveal the unique compositional signatures that distinguish cell-wall material from other whole-cell components (Fig. 2). Cell-wall ^{13}C and ^{15}N spectra provide the total compositional pools of peptidoglycan, with its five amino acids and disaccharide building blocks, and teichoic acid. The carbon spectrum accounted for the corresponding set of anticipated chemical shifts and the nitrogen spectrum immediately revealed the highly cross-linked nature of the material (as amides) with little detectable amine intensity. Selective NMR experiments aided accurate spectral assignments and one-bond REDOR experiments confirmed that all α-carbons assigned in the spectrum exhibited complete dephasing by ^{15}N resulting from peptide bond C-N pairs (Figs. 3 and 4). Although REDOR is often used and appreciated for its robustness and ability to measure accurate long-range distances in selectively labeled systems with isolated spin pairs such as in protein complexes and drug-cell-wall complexes, the REDOR approach is powerful in its ability to serve as a spectroscopic filter. This is shown in Figs. 3 and 4 to quantify the extent of one-bond C-N pairs, for example. Whole-cell ^{13}C and ^{15}N spectra are more complex including contributions from all proteins, nucleic acids, and biomolecules in the cell, including the cell wall. Yet, we hypothesized that we could detect changes in cell-wall composition by whole-cell NMR through the cell-wall polysaccharide spectral signatures. The most straightforward test of this hypothesis is illustrated by the comparative ^{13}C CPMAS spectra of whole cells and protoplasts in which the majority of the cell wall is stripped away from the cells after lysostaphin treatment (Fig. 6). This revealed the major contribution of polysaccharides to cell walls that are not representative of other cellular pools and the ability to monitor the relative amount of cell wall among whole-cell samples through a ^{13}C CPMAS spectrum.

A major motivation for our work is to ultimately examine emerging antibiotic candidates and evaluate their modes of action in whole cells using the most informative panel of whole-cell and cell-wall NMR approaches, particularly for *S. aureus* and other Gram-positive pathogens. In this contribution, we discovered that a whole-cell NMR spectrum of fosfomycin-treated cells could reveal a decrease in cell-wall content. In comparison, treatment with the protein synthesis inhibitor chloramphenicol resulted in an altered compositional balance where the cell-wall spectral contributions were increased relative to untreated cells, while cellular pools associated with proteins were decreased because cytoplasmic protein pools were not replenished during antibiotic treatment. Thus, in addition to providing a spectral snapshot of cell-wall content, we are also able to capture global changes in carbon and nitrogen cellular metabolism through the whole-cell NMR spectra. This latter example, in particular, emphasizes the applicability of solid-state NMR to examine the influence of other perturbations on overall carbon pools within intact cellular assemblies. This approach is general, does not require selective labeling strategies, and can be implemented to examine cell-wall alterations, such as those due to antibiotics, genetic mutations, or other environmental conditions. In addition, future work with ^{31}P NMR can be used to further dissect cell-wall spectra and to distinguish the peptidoglycan sugars as arising from either peptidoglycan or teichoic acid components of the cell wall.

AUTHOR CONTRIBUTIONS

All authors contributed to the design of the research and data analysis. R.N., J.A.H.R., and D.M.R. performed experiments, and R.N. and L.C. composed the manuscript.

ACKNOWLEDGMENTS

We acknowledge Xiaoxue Zhou and Lydia-Marie Joubert and the Stanford Cell Sciences Imaging Facility for access to and assistance with electron microscopy.

R.N. is the recipient of the Lundbeck Foundation Postdoctoral Fellowship. L.C. gratefully acknowledges support from the National Institutes of Health's Director's New Innovator Award (No. DP2OD007488), Stanford University, the Stanford Terman Fellowship, and the Hellman Faculty Scholar Award.

REFERENCES

1. Vollmer, W., D. Blanot, and M. A. de Pedro. 2008. Peptidoglycan structure and architecture. *FEMS Microbiol. Rev.* 32:149–167.
2. Typas, A., M. Banzhaf, …, W. Vollmer. 2012. From the regulation of peptidoglycan synthesis to bacterial growth and morphology. *Nat. Rev. Microbiol.* 10:123–136.
3. Wright, G. D. 2012. Antibiotics: a new hope. *Chem. Biol.* 19:3–10.
4. Hao, H., G. Cheng, …, Z. Yuan. 2012. Inhibitors targeting on cell wall biosynthesis pathway of MRSA. *Mol. Biosyst.* 8:2828–2838.
5. Schneider, T., and H. G. Sahl. 2010. An oldie but a goodie—cell wall biosynthesis as antibiotic target pathway. *Int. J. Med. Microbiol.* 300:161–169.
6. Lowy, F. D. 1998. *Staphylococcus aureus* infections. *N. Engl. J. Med.* 339:520–532.
7. Klevens, R. M., M. A. Morrison, …, S. K. Fridkin. 2007. Invasive methicillin-resistant *Staphylococcus aureus* infections in the United States. *JAMA.* 298:1763–1771.
8. Fox, J. L. 2014. Second MRSA antibiotic reaches the market. *Nat. Biotechnol.* 32:972.
9. Wright, G. D., and H. Poinar. 2012. Antibiotic resistance is ancient: implications for drug discovery. *Trends Microbiol.* 20:157–159.
10. Kahan, F. M., J. S. Kahan, …, H. Kropp. 1974. The mechanism of action of fosfomycin (phosphonomycin). *Ann. N. Y. Acad. Sci.* 235:364–386.
11. Tipper, D. J., and J. L. Strominger. 1965. Mechanism of action of penicillins: a proposal based on their structural similarity to acyl-D-alanyl-D-alanine. *Proc. Natl. Acad. Sci. USA.* 54:1133–1141.
12. Yocum, R. R., J. R. Rasmussen, and J. L. Strominger. 1980. The mechanism of action of penicillin. Penicillin acylates the active site of *Bacillus stearothermophilus* D-alanine carboxypeptidase. *J. Biol. Chem.* 255:3977–3986.
13. Brown, S., J. P. Santa Maria, Jr., and S. Walker. 2013. Wall teichoic acids of Gram-positive bacteria. *Annu. Rev. Microbiol.* 67:313–336.
14. Navarre, W. W., and O. Schneewind. 1999. Surface proteins of Gram-positive bacteria and mechanisms of their targeting to the cell wall envelope. *Microbiol. Mol. Biol. Rev.* 63:174–229.
15. Cegelski, L., S. J. Kim, …, J. Schaefer. 2002. Rotational-echo double resonance characterization of the effects of vancomycin on cell wall synthesis in *Staphylococcus aureus*. *Biochemistry.* 41:13053–13058.
16. Kim, S. J., L. Cegelski, …, J. Schaefer. 2008. Oritavancin exhibits dual mode of action to inhibit cell-wall biosynthesis in *Staphylococcus aureus*. *J. Mol. Biol.* 377:281–293.
17. Glauner, B. 1988. Separation and quantification of muropeptides with high-performance liquid chromatography. *Anal. Biochem.* 172:451–464.
18. Kim, S. J., L. Cegelski, …, J. Schaefer. 2002. Rotational-echo double resonance characterization of vancomycin binding sites in *Staphylococcus aureus*. *Biochemistry.* 41:6967–6977.
19. Cegelski, L., D. Steuber, …, J. Schaefer. 2006. Conformational and quantitative characterization of oritavancin-peptidoglycan complexes in whole cells of *Staphylococcus aureus* by in vivo ^{13}C and ^{15}N labeling. *J. Mol. Biol.* 357:1253–1262.
20. Kim, S. J., L. Cegelski, …, J. Schaefer. 2006. Structures of *Staphylococcus aureus* cell-wall complexes with vancomycin, eremomycin, and chloroeremomycin derivatives by $^{13}C^{19}F$ and $^{15}N^{19}F$ rotational-echo double resonance. *Biochemistry.* 45:5235–5250.
21. Kim, S. J., S. Matsuoka, …, J. Schaefer. 2008. Vancomycin derivative with damaged D-Ala-D-Ala binding cleft binds to cross-linked peptidoglycan in the cell wall of *Staphylococcus aureus*. *Biochemistry.* 47:3822–3831.
22. Kim, S. J., and J. Schaefer. 2008. Hydrophobic side-chain length determines activity and conformational heterogeneity of a vancomycin derivative bound to the cell wall of *Staphylococcus aureus*. *Biochemistry.* 47:10155–10161.
23. Kim, S. J., K. S. E. Tanaka, …, J. Schaefer. 2013. Locations of the hydrophobic side chains of lipoglycopeptides bound to the peptidoglycan of *Staphylococcus aureus*. *Biochemistry.* 52:3405–3414.
24. Cho, H., T. Uehara, and T. G. Bernhardt. 2014. Beta-lactam antibiotics induce a lethal malfunctioning of the bacterial cell wall synthesis machinery. *Cell.* 159:1300–1311.
25. Zhou, X., and L. Cegelski. 2012. Nutrient-dependent structural changes in *S. aureus* peptidoglycan revealed by solid-state NMR spectroscopy. *Biochemistry.* 51:8143–8153.
26. Tong, G., Y. Pan, …, J. Schaefer. 1997. Structure and dynamics of pentaglycyl bridges in the cell walls of *Staphylococcus aureus* by ^{13}C-^{15}N REDOR NMR. *Biochemistry.* 36:9859–9866.
27. Schaefer, J., and T. Gullion. 1989. Development of REDOR rotational-echo double-resonance NMR. *J. Magn. Reson.* 81:196–200.
28. Jaroniec, C. P., B. A. Tounge, …, R. G. Griffin. 2001. Frequency selective heteronuclear dipolar recoupling in rotating solids: accurate ^{13}C-^{15}N distance measurements in uniformly ^{13}C,^{15}N-labeled peptides. *J. Am. Chem. Soc.* 123:3507–3519.
29. Li, Y., B. J. Wylie, and C. M. Rienstra. 2006. Selective refocusing pulses in magic-angle spinning NMR: characterization and applications to multi-dimensional protein spectroscopy. *J. Magn. Reson.* 179:206–216.
30. McDermott, A., T. Polenova, …, G. T. Montelione. 2000. Partial NMR assignments for uniformly ^{13}C, ^{15}N-enriched BPTI in the solid state. *J. Biomol. NMR.* 16:209–219.
31. Takegoshi, K., S. Nakamura, and T. Terao. 2001. ^{13}C-^{1}H dipolar-assisted rotational resonance in magic-angle spinning NMR. *Chem. Phys. Lett.* 344:631–637.
32. Cegelski, L., and J. Schaefer. 2005. Glycine metabolism in intact leaves by in vivo ^{13}C and ^{15}N labeling. *J. Biol. Chem.* 280:39238–39245.
33. Rudin, L., J. E. Sjöström, …, L. Philipson. 1974. Factors affecting competence for transformation in *Staphylococcus aureus*. *J. Bacteriol.* 118:155–164.
34. Grif, K., M. P. Dierich, …, F. Allerberger. 2001. In vitro activity of fosfomycin in combination with various antistaphylococcal substances. *J. Antimicrob. Chemother.* 48:209–217.
35. Gisin, J., A. Schneider, …, C. Mayer. 2013. A cell wall recycling shortcut that bypasses peptidoglycan de novo biosynthesis. *Nat. Chem. Biol.* 9:491–493.
36. Contreras, A., M. Barbacid, and D. Vazquez. 1974. Binding to ribosomes and mode of action of chloramphenicol analogs. *Biochim. Biophys. Acta.* 349:376–388.
37. Thompson, J., M. O'Connor, …, A. E. Dahlberg. 2002. The protein synthesis inhibitors, oxazolidinones and chloramphenicol, cause extensive translational inaccuracy in vivo. *J. Mol. Biol.* 322:273–279.

38. Xaplanteri, M. A., A. Andreou, …, D. L. Kalpaxis. 2003. Effect of polyamines on the inhibition of peptidyltransferase by antibiotics: revisiting the mechanism of chloramphenicol action. *Nucleic Acids Res.* 31:5074–5083.

39. Vollmer, W., and S. J. Seligman. 2010. Architecture of peptidoglycan: more data and more models. *Trends Microbiol.* 18:59–66.

40. de Jonge, B. L., Y. S. Chang, …, A. Tomasz. 1992. Peptidoglycan composition of a highly methicillin-resistant *Staphylococcus aureus* strain. The role of penicillin binding protein 2A. *J. Biol. Chem.* 267:11248–11254.

41. Boneca, I. G., Z. H. Huang, …, A. Tomasz. 2000. Characterization of *Staphylococcus aureus* cell wall glycan strands, evidence for a new β-*n*-acetylglucosaminidase activity. *J. Biol. Chem.* 275:9910–9918.

42. Patti, G. J., J. Chen, and M. L. Gross. 2009. Method revealing bacterial cell-wall architecture by time-dependent isotope labeling and quantitative liquid chromatography/mass spectrometry. *Anal. Chem.* 81:2437–2445.

43. De Lencastre, H., S. W. Wu, …, A. Tomasz. 1999. Antibiotic resistance as a stress response: complete sequencing of a large number of chromosomal loci in *Staphylococcus aureus* strain COL that impact on the expression of resistance to methicillin. *Microb. Drug Resist.* 5:163–175.

44. Sieradzki, K., M. G. Pinho, and A. Tomasz. 1999. Inactivated pbp4 in highly glycopeptide-resistant laboratory mutants of *Staphylococcus aureus*. *J. Biol. Chem.* 274:18942–18946.

45. Kern, T., M. Giffard, …, J. P. Simorre. 2010. Dynamics characterization of fully hydrated bacterial cell walls by solid-state NMR: evidence for cooperative binding of metal ions. *J. Am. Chem. Soc.* 132:10911–10919.